Characterizing Aerodynamic Damping of a Supersonic Missile with CFD

Andrew Shelton,[*] Christopher Martin[†]

Leidos, Inc., Eglin AFB, Florida, 32542, USA

and

Walter Silva[‡]

Aeroelasticity Branch, NASA Langley Research Center, Hampton, Virginia, 23681, USA

Time accurate solutions of the Euler and Navier–Stokes equations are used as an approach to elucidate aerodynamic coefficients that include rigid body motion effects. The Army-Navy Finner geometry is used for workflow development due to its simple shape, inexpensive grid generation, and available literature that include aerodynamic damping derivatives obtained from flight test, wind tunnel tests, and computational fluid dynamics. Supersonic conditions for pitch and roll damping include angles of attack up to 90 deg.

Aerodynamic responses due to rigid body maneuvers with prescribed wind incidence angles and body rates are computed using the DoD CREATE Kestrel and NASA FUN3D flow solvers. First, reference numerical and experimental results provide validation of aerodynamic damping terms computed by traditional periodic motion in roll and pitch. Next, individual, impulse motion inputs provide the canonical responses for general input-output modeling based on classical superposition and convolution concepts. Finally, simultaneous impulse excitation of all inputs provides an efficient system identification training scenario for accurate aerodynamic model construction in state space via the NASA System/Observer/Controller Identification Toolbox.

Nomenclature

$h_{i,j}$	=	impulse response for output i due to input j
k	=	reduced frequency
$f_i(t)$	=	schedule for angle/rate i
p, q, r	=	body angular velocity components (deg/s)
p_t	=	stagnation pressure (lb/ft^2)
t	=	time (s)
u, v, w	=	relative wind velocity components (ft/s)
u, x, y	=	state space model control, state, and output vectors
x, y, z	=	position components (ft)
A, B, C, D	=	state space model system dynamics, control, output, and transmission matrices
C_A, C_S, C_N	=	axial, side, and normal aerodynamic force coefficients
C_l, C_m, C_n	=	rolling, pitching, and yawing aerodynamic moment coefficients

---

[*]Senior CFD Researcher, Senior Member, AIAA
[†]CFD Researcher, Senior Member, AIAA
[‡]Senior Research Scientist, Associate Fellow, AIAA

C_{i_j}	=	derivative of aerodynamic force/moment coefficient i with respect to angle/rate j
D	=	missile reference diameter (in)
L	=	missile reference length, $10D$ (in)
M	=	Mach number
N	=	number of time steps
Re_D	=	Reynolds number based on diameter
T	=	convective time scale L/V (s)
T_t	=	stagnation temperature (deg R)
$S_{i,j}$	=	step response for output i due to input j
U	=	state space model control input matrix
V	=	freestream wind velocity magnitude (ft/s)
Y	=	state space model Markov parameter matrix
α, β	=	angle of attack and angle of slip (deg)
$\alpha_{\text{t}}, \phi_{\text{a}}$	=	total angle of attack and aerodynamic roll angle (deg)
δ	=	unit impulse
μ	=	unit step
ϕ, θ, ψ	=	Euler angles roll, pitch, yaw (deg)
τ	=	time origin for motion start (s)
ω	=	frequency (Hz)
Ω	=	dimensionless spin rate
Δt	=	time step size T/N (s)
$(\cdot)_0$	=	value at reference steady state, $t = 0$
$\dot{(\cdot)}$	=	time rate of change
$\bar{(\cdot)}$	=	weighted time average or observer-modified state space matrices

I.   Introduction

I.A.   Problem Statement

Accurate prediction of aerodynamic forces and moments is crucial for aircraft performance assessment, including stability to both static and dynamic flight disturbances over a wide range of angles of attack. Aerodynamic load hysteresis occurs at all nonzero motion frequencies, and is fundamentally related to the phase lag of fluid advection to relative input motion. This information is traditionally captured within aerodynamic models by damping derivatives as discussed by Jenkins.[1] Mathematically, these derivatives appear by a Taylor series expansion on the aerodynamic coefficients with respect the wind incidence angles, their rates, and the body rotation rates

$$
\begin{aligned}
C_\ell(t) = {} & C_{\ell_0} + C_{\ell_\alpha}(\alpha - \alpha_0) + C_{\ell_\beta}(\beta - \beta_0) \\
& + C_{\ell_{\dot\alpha}} \frac{\dot\alpha D}{2V} + C_{\ell_{\dot\beta}} \frac{\dot\beta D}{2V} \\
& + C_{\ell_p} \frac{pD}{2V} + C_{\ell_q} \frac{qD}{2V} + C_{\ell_r} \frac{rD}{2V} + \cdots,
\end{aligned}
\tag{1}
$$

where $\ell = A, S, N, l, m, n$. Each of the coefficients is a function of the reference steady state as $C_{\ell_j}(\alpha_0, \beta_0, \dots)$ with $j = \alpha, \beta, p, q, r$. Component dependencies are typically reduced for longitudinal quantities $\ell = N, m$ as

$$
C_\ell(t) = C_{\ell_0} + C_{\ell_\alpha}(\alpha - \alpha_0) + C_{\ell_{\dot\alpha}} \frac{\dot\alpha D}{2V} + C_{\ell_q} \frac{qD}{2V},
\tag{2}
$$

and for lateral quantities $\ell = S, l, n$ as

$$
C_\ell(t) = C_{\ell_0} + C_{\ell_\beta}(\beta - \beta_0) + C_{\ell_{\dot\beta}} \frac{\dot\beta D}{2V} + C_{\ell_p} \frac{pD}{2V} + C_{\ell_r} \frac{rD}{2V}.
\tag{3}
$$

Alternatively, if an airframe continuously rolls, it may be desirable to work with total angle of attack, α_t, and aerodynamic roll angle, ϕ_a, as independent variables. In this case

$$C_\ell(t) = C_{\ell_0} + C_{\ell_{\alpha_\mathrm{t}}}(\alpha_\mathrm{t} - \alpha_{\mathrm{t}_0}) + C_{\ell_{\phi_\mathrm{a}}}(\phi_\mathrm{a} - \phi_{\mathrm{a}_0}) + C_{\ell_{\dot{\alpha}_\mathrm{t}}}\frac{\dot{\alpha}_\mathrm{t} D}{2V} + C_{\ell_p}\frac{pD}{2V}, \tag{4}$$

with $C_{\ell_j}(\alpha_{\mathrm{t}_0}, \phi_{\mathrm{a}_0}, \ldots)$. With the availability and affordability of unsteady computational fluid dynamics (CFD) that includes grid motion, research has recently focused on exploiting CFD for computing the aerodynamic derivatives in the above formulas.[2–5] This work aims to determine the damping terms in Equation 2 and Equation 4 for a supersonic missile by considering various motion specifications as aerodynamic model training maneuvers within a CFD-based process.

I.B.   Scope and Objectives

Requiring even simple time-dependent prescribed motions to excite the damping terms of interest compounds the difficulties and expense of both physical and numerical aerodynamic testing. Uselton & Uselton[6] describe a wind tunnel test mechanism with an oscillating air system to displace a missile model about its pitch axis. Bhagwandin & Sahu[7] performed CFD studies of the corresponding harmonic pitch motion and obtained good results for the computed pitch damping. Jenke[8] described a wind tunnel test mechanism with a spinning balance with air jets to displace the model about its roll axis. Bhagwandin[9] performed CFD studies of the corresponding constant roll rate motion and obtained good results for the computed roll damping. In this work, we repeat those simulations for validation of the basic, prescribed periodic motion, CFD workflow.

In the interest of developing a more economical CFD-based training process for aerodynamic modeling, we then turn our attention to the impulse response aerodynamics. With an inherently wide frequency content, this canonical response completely characterizes the system about a reference flight condition state and allows time-dependent aerodynamic loads prediction due to nearby arbitrary motion. System identification concepts provide generalization of the impulse response approach for simultaneous inputs and outputs. While more sophisticated to setup and analyze, this approach promises fewer and shorter CFD runs to generate aerodynamic damping coefficients. There are two main objectives of this paper: (1) summarize the ingredients necessary to prescribe 3D motion input and to analyze the aerodynamic output for damping; and (2) demonstrate application of these processes to a reference missile configuration using currently available CFD tools for baseline workflow characterization.

For the first goal, we provide the variety of mathematical details involved in unsteady motion setup and aerodynamic analysis. A description the equations of motion, aerodynamic derivatives, and pure motions in pitch and roll provides the basic information required to repeat the reference wind tunnel and reference numerical scenarios. Additionally, a review of linear time-invariant system dynamics concepts emphasizes the connection of impulse response to state space model and lead to the fundamental algorithms of the System/Observer/Controller Identification Toolbox (SOCIT).[10]

For the second goal, we setup and exercise the Kestrel and FUN3D flow solvers with various prescribed motions to compute the documented aerodynamic damping for Army-Navy Finner at a Mach number near $M \approx 2$ and angles of attack $0 \leq \alpha \leq 90$ deg. We summarize the reference flow conditions, reference airframe geometry, mesh generation, and flow solver strategy and settings. We report the aerodynamic results for rigid body CFD solution response to various types of motion, from constant rate roll and harmonic pitch to simultaneous impulse in all wind incidence angles and body rates according to Walsh function time schedules.

II.   Computational Setting

II.A.   Coordinate Frames and Equations of Motion

Figure 1 shows a generic missile and associated vector components of loads and kinematic rates. The relative wind and right-handed body rotation rates are in a CFD-centric body axis

- $(u, p) > 0$ along x-tail,

- $(v, q) > 0$ along y-right, and

- $(w, r) > 0$ along z-up.

According to tradition, aerodynamic force coefficients are

- Axial force, $C_A > 0$ along x-tail,

- Side force, $C_S > 0$ along y-right,

- Normal force, $C_N > 0$ along z-up,

while aerodynamic right-handed moment coefficients are

- Rolling moment, $C_l > 0$ along x-nose,

- Pitching moment, $C_m > 0$ along y-right, and

- Yawing moment, $C_n > 0$ along z-down.

The angle of attack and angle of slip are in terms of the relative wind components

$$
\begin{aligned}
\alpha &= \tan^{-1}(w/u), \\
\beta &= \sin^{-1}(-v/V),
\end{aligned}
\tag{5}
$$

while for a rolling airframe, the total angle of attack and aerodynamic roll angle are

$$
\begin{aligned}
\alpha_{\mathrm{t}} &= \cos^{-1}(\cos\alpha \cos\beta), \\
\phi_{\mathrm{a}} &= \tan^{-1}(-\tan\beta/\sin\alpha).
\end{aligned}
\tag{6}
$$

In this work, motion prescription operates in the fixed CFD reference frame, which at time $t = 0$ is aligned with the body frame (x-tail, y-right, z-up). User-desired schedules for wind inclination angles (body translation rates) and body rotation rates take the form

$$
\begin{aligned}
\alpha(t) &= \alpha_0 + f_\alpha(t),\ \beta(t) = \beta_0 + f_\beta(t), \\
p(t) &= p_0 + f_p(t),\ q(t) = q_0 + f_q(t),\ r(t) = r_0 + f_r(t).
\end{aligned}
\tag{7}
$$

The mass center coordinates and orientation of the flight vehicle relative to the fixed CFD reference frame are determined by integrating the equations of motion[11–13]

$$
\begin{aligned}
\frac{\mathrm{d}}{\mathrm{d}t}\begin{Bmatrix} x \\ y \\ z \end{Bmatrix} &= R^{-1}(t)\begin{Bmatrix} u(t) \\ v(t) \\ w(t) \end{Bmatrix}, \\
\frac{\mathrm{d}}{\mathrm{d}t}\begin{Bmatrix} \phi \\ \theta \\ \psi \end{Bmatrix} &= T^{-1}(t)\begin{Bmatrix} p(t) \\ q(t) \\ r(t) \end{Bmatrix},
\end{aligned}
\tag{8}
$$

with zero initial conditions. Accounting for a constant imposed wind vector in the fixed reference frame, the apparent velocity relative to the flight vehicle is

$$
\begin{Bmatrix} u(t) \\ v(t) \\ w(t) \end{Bmatrix} = R(t)\,V\begin{Bmatrix} \cos\alpha_0 \cos\beta_0 \\ -\sin\beta_0 \\ \sin\alpha_0 \cos\beta_0 \end{Bmatrix} - V\begin{Bmatrix} \cos\alpha(t)\cos\beta(t) \\ -\sin\beta(t) \\ \sin\alpha(t)\cos\beta(t) \end{Bmatrix}.
\tag{9}
$$

The rotation matrix from the fixed reference frame to the body frame follows the traditional "Yaw-Pitch-Roll" ordering

$$
R(t) = R_x(\phi(t))\,R_y(\theta(t))\,R_z(\psi(t)),
\tag{10}
$$

and the transformation matrix from the Euler angle frame (intermediate, moving states) to the body frame is

$$
T(t) = \left[\begin{Bmatrix} 1 \\ 0 \\ 0 \end{Bmatrix},\ R_x(\phi(t))\begin{Bmatrix} 0 \\ 1 \\ 0 \end{Bmatrix},\ R_x(\phi(t))R_y(\theta(t))\begin{Bmatrix} 0 \\ 0 \\ 1 \end{Bmatrix}\right].
\tag{11}
$$

Finally, the individual rotation matrices for roll, pitch, yaw are

$$R_x(\phi) = \begin{bmatrix} 1 & 0 & 0 \\ 0 & \cos\phi & -\sin\phi \\ 0 & \sin\phi & \cos\phi \end{bmatrix}, R_y(\theta) = \begin{bmatrix} \cos\theta & 0 & \sin\theta \\ 0 & 1 & 0 \\ -\sin\theta & 0 & \cos\theta \end{bmatrix}, R_z(\psi) = \begin{bmatrix} \cos\psi & -\sin\psi & 0 \\ \sin\psi & \cos\psi & 0 \\ 0 & 0 & 1 \end{bmatrix}. \qquad (12)$$
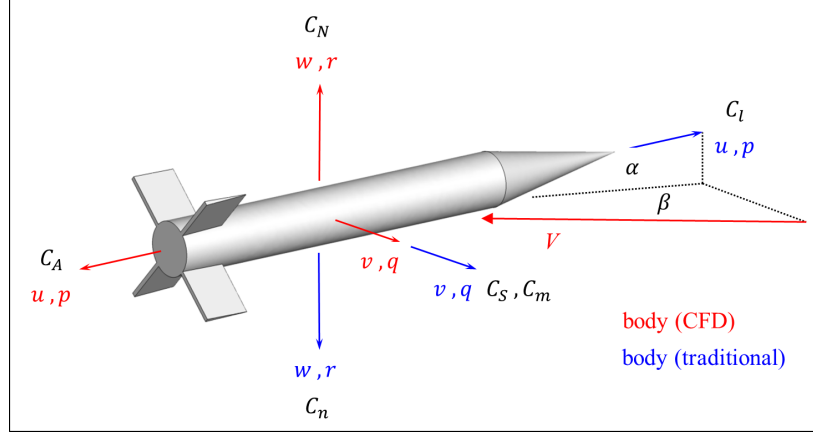

Figure 1: Axes systems.

II.B. Reference Experimental Conditions and Configuration

Experimentally-determined aerodynamic pitch and roll damping data from the Arnold Engineering Development Center (AEDC) Supersonic Wind Tunnel facility[6,8] are used to validate the current numerical results. Table 1 summarizes the conditions from those tests that are used in this work. Figure 2 shows the OML of the Army-Navy Finner geometry used in the test articles: a basic projectile with $L/D = 10$ overall fineness, $D \times D$ planform wedge section fins, and a $2.836D$ length conical nose.

The wind tunnel technique for pitch damping due to Uselton & Uselton[6] is summarized as

> "The high-alpha pitch-damping test mechanism utilizes a small-amplitude one-degree-of freedom cross-flexure balance which is supported by a strut and sting that can be manually adjusted to provide minimum aerodynamic interference and angles of attack ranging from -15 to 90 deg. A strain-gage bridge is located on the flexures to provide a voltage proportional to angular displacement. An oscillating-air system was used to displace the model. The driving force was obtained from a high-pressure air supply which was adjusted to the pressure level necessary to overcome the damping moment. The model was oscillated by two air jets that were regulated by a remotely controlled servovalve oscillating at the natural frequency of the model and balance system. The driving force could be stopped abruptly by a solenoid valve and data recorded as the amplitude decreased."

The corresponding computational exercise applies constant amplitude and frequency harmonic motion in pitch according to the process in §III.B.

The wind tunnel technique for roll damping due to Jenke[8] is summarized as:

> "The high-alpha missile roll-damping test mechanism is a free-spin system. A six-component balance is supported by a strut that can be manually set in 6-deg increments to provide various prebend angles. These manual settings along with the tunnel pitch mechanism provide an angle-of-attack range from -5 to 90 deg. The balance supports an adapter with three ball bearings, and the model is mounted directly to the bearings. An air-operated brake is located on the front of the adapter and is used to stop model rotation. The brake as well as a mechanical lock can be used to obtain static force coefficients at zero spin rate. Roll-damping data are obtained as the model spins down after it is spun up by high pressure air jets impinging on the fins. The rotational speed, roll position, and roll direction are computed from the electrical pulses produced

by a ring with alternating reflective and nonreflective surfaces passing three internally mounted infrared-emitting diodes and phototransistors."

The corresponding computational exercise applies constant rate of motion in roll according to the process in §III.A.

Table 1: Wind Tunnel Test Parameters

Quantity	Units	Pitch[6]	Roll[8]
D	in	1.25	1.80
M	–	1.96	2.49
Re_D	–	1.87×10^5	1.86×10^5
V	ft/s	1698	1929
T_t	deg R	522	560
P_t	lb/ft^2	1022	936
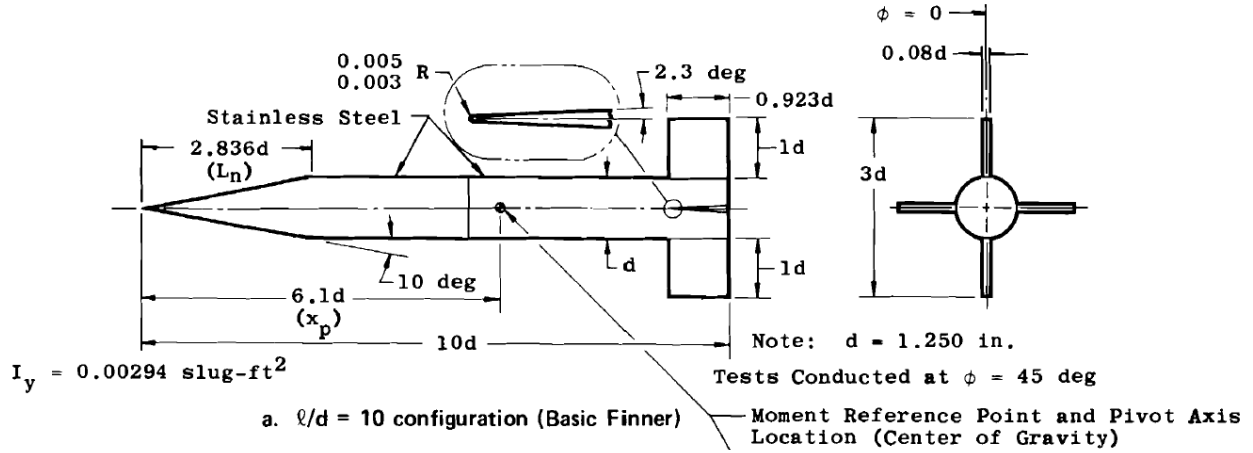
Figure 2: Wind Tunnel Model Details.[6]

II.C. Geometry and Meshing

CREATE-MG Capstone[14] is employed to construct all geometry and unstructured meshes. The model orientation is the typical CFD convention with x-tail, y-right, z-up, and the origin at the nose. For computational economy of mesh generation and some pitch plane simulations, only a half-body geometry is constructed with fins arranged in a "×" configuration symmetric relative to the xz-plane. Meshes are scaled to the proper D according to comparison wind tunnel test and mirrored as required for non-pitch plane motion.

OML construction begins with fin cross section leading and trailing edge points to establish a chord of $c/D = 1$ and thickness $t/D = 0.1$. Fin wedge volume then proceeds according to a point, line, face, volume build-up process. The root airfoil plane is intentionally placed at a location inside the body radius. A leading edge fillet is added with $r/D = 0.005$. The fin is copied and the pair rotated into "×" configuration. Similarly, the nose build-up uses leading and trailing edge points connected with straight lines. A leading edge fillet is added with $r/D = 0.005$. The profile is then split and the upper half revolved to form a blunted cone. The missile body is a simple solid primitive cylinder. The nose, body, and two tail fins are merged into a single body using Boolean addition.

The air volume around the OML consists inner and outer boxes of dimension ($11D$, $2D$, $4D$) and ($120D$, $60D$, $120D$), respectfully, aligned with the half-body OML on the xz-plane of symmetry and centered on the OML midpoint in the x- and z-axes. These volumes are merged using an "unregularized" Boolean union. Finally, the OML is removed from the air volume by Boolean subtraction.

American Institute of Aeronautics and Astronautics

Table 2 summarizes Capstone meshing parameters. For viscous simulations, the mesh wall spacing provides steady state solutions with $y^+ < 0.5$. Note that total cell count refers to a full 3D (mirrored half-body) mesh. Figure 3 provides example visualizations of the coarse mesh with boundary layer.

Table 2: Capstone Meshing Parameters (units based on D)

Quantity	Coarse	Medium	Fine
Global size	480	240	120
Minimum size	0.004	0.002	0.001
Increment	1.125	1.125	1.125
Curvature based sizing	40	75	150
Topos, OML volume	0.24	0.12	0.06
Topos, OML surface	0.08	0.04	0.02
Topos, OML edge	0.008	0.004	0.002
BL wall	0.0001	0.0001	0.0001
BL layers	20	20	20
BL rate	1.125	1.125	1.125
Cells w/ BL	11,072,348	n/a	65,097,020
Cells w/o BL	8,091,797	18,111,449	n/a

II.D.   Flow Solution

The flow solvers for this work are DoD CREATE-AV Kestrel v6.2.2[15] and NASA FUN3D v12.7.[16] Both are exercised for solution of the Euler equations and the Navier-Stokes equations with Delayed Detached Eddy Simulation turbulence model formulation.

A steady state solution is computed for each unique $(V, P_t, T_t, \alpha_0, \beta_0)$ initial condition. Both flow solvers use local time stepping for 500 steps, during which the CFL number is ramped $0.1 - 20$ over the first 100 steps and the spatial accuracy is ramped over the first 200 steps. Unsteady solutions are restarted from the steady pre-solution and driven by subsequent whole-mesh rigid body motion. The temporal evolution strategy for Kestrel uses 5 Newton subiterations while FUN3D uses the temporal error control feature on dual timestepping with 16 psuedo-steps at a CFL = 10. The physical timestep is based on recommended practice[17] as $\Delta t = T/N$, where $N \geq 100$ and the convective time scale based on body length and freestream velocity is $T = L/V$. The first rigid body motion in all unsteady cases starts at $\tau = 2T$ and motion lasts no less than $t_{\text{final}} - \tau = 6T$. Other temporal resolution checks follow: for a wake shedding frequency of $\text{St} = fD/V = 0.2$, $N_{\text{St}} \geq 50$ steps per cycle and for harmonic motion of less than 6 cycles in the motion period, $N_{\text{HM}} \geq 50$ steps per cycle.

For a user-desired discrete time list $(t_0, t_1, \ldots, t_K)$ and motion schedule, Equation (7), the Matlab function `ode45` is employed to solve Equation (8) to obtained a discrete time history of the vehicle mass center coordinates (x, y, z) and orientation (ϕ, θ, ψ). Although both flow solvers have functionality to interpolate position and orientation data along an arbitrary, monotonically increasing time list, all motion scenarios in this work simply take $t_k = k\Delta t$, with $k = 0, \ldots, K$, where K an integer multiple of N, to avoid any error or unintended splining.

The motion input for Kestrel uses the coordinates and orientation angles directly. The motion input for FUN3D embeds them in a 4×4 transformation matrix that maps from the moving body coordinates to the fixed reference frame as the sequence "Origin to cg – Rotate – Origin to nose – Translate"

$$\begin{Bmatrix} x \\ y \\ z \\ 1 \end{Bmatrix}_{\text{ref}} = X(t)\, C\, Q(t)\, C^{-1} \begin{Bmatrix} x \\ y \\ z \\ 1 \end{Bmatrix}_{\text{body}}, \tag{13}$$
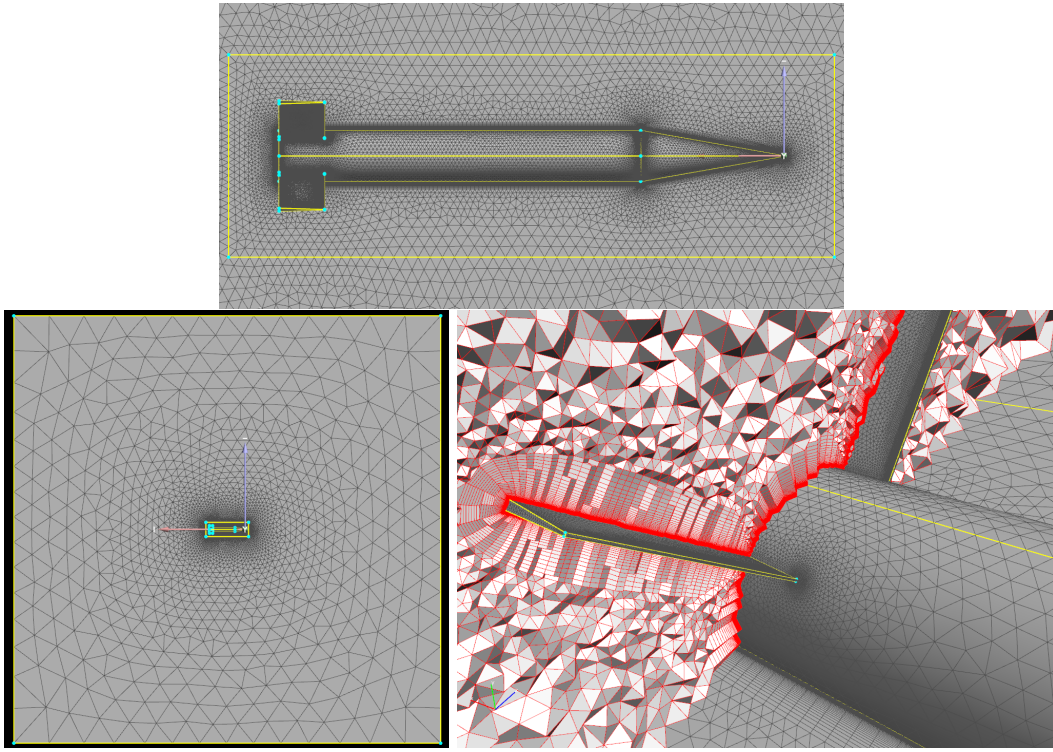
Figure 3: Coarse mesh: detail near OML showing near-body refinement box and boundary layer (top), full domain xz plane (bottom left), detail near tail fins showing boundary layer and fin edge refinements (bottom right).

where

$$
Q(t) = \begin{bmatrix} & & & 0 \\ & R^{-1}(t) & & 0 \\ & & & 0 \\ 0 & 0 & 0 & 1 \end{bmatrix}, \quad
X(t) = \begin{bmatrix} 1 & 0 & 0 & x(t) \\ 0 & 1 & 0 & y(t) \\ 0 & 0 & 1 & z(t) \\ 0 & 0 & 0 & 1 \end{bmatrix}, \quad
C = \begin{bmatrix} 1 & 0 & 0 & x_{\mathrm{cg}} \\ 0 & 1 & 0 & y_{\mathrm{cg}} \\ 0 & 0 & 1 & z_{\mathrm{cg}} \\ 0 & 0 & 0 & 1 \end{bmatrix}.
\tag{14}
$$

III. Validation of Periodic Motion

III.A. Forced Continuous Roll

Consider pure rolling motion with fixed total angle of attack $\alpha_{\mathrm{t}} = \cos^{-1}(\cos\alpha\cos\beta)$ and linearly time-varying aerodynamic roll angle $\phi_{\mathrm{a}} = \tan^{-1}(-\tan\beta/\sin\alpha) = pt$. Evaluating Equation (1) at some (small) fixed $\Delta\phi_{\mathrm{a}}$ from two different rates p yields

$$
\Delta C_l = C_{l_p}\Delta\Omega,
\tag{15}
$$

with the dimensionless spin rate

$$
\Omega = \frac{pD}{2V}.
\tag{16}
$$

Averaging the response with respect to roll angle as

$$
\bar{C}_l = \frac{1}{\phi_b - \phi_a}\int_{\phi_a}^{\phi_b} C_l\,\mathrm{d}\phi_{\mathrm{a}},
\tag{17}
$$

provides a means to compute the roll damping moment

$$
\bar{C}_{l_p} = \frac{\Delta\bar{C}_l}{\Delta\Omega}.
\tag{18}
$$

The integration range $\phi_b - \phi_a = 2\pi n/jp$ covers $n \geq 1$ integer number of periods of airframe symmetry (*e.g.*, 90 deg for $j = 4$ fins) and typically starts no sooner than the third period. Aerodynamic components are reported in the maneuver plane system, obtained via the transformation $R_x(\phi_a)$.

Example CFD solutions apply this scenario for comparing roll damping with reference wind tunnel[8] and numerical[9] results. The motion prescription for forced continuous rolling at constant total angle of attack is

$$
\begin{aligned}
f_\alpha(t) &= \tan^{-1}\left(\cos\phi_a(t)\tan\alpha_t(t)\right), \\
f_\beta(t) &= -\sin^{-1}\left(\sin\phi_a(t)\sin\alpha_t(t)\right), \\
f_p(t) &= (2V\Omega/D)\,\mu(t-\tau), \\
f_q(t) &= f_r(t) = 0,
\end{aligned}
\tag{19}
$$

with $\alpha_t(t) = \alpha_0$ and $\phi_a(t) = \phi(t)$. Two dimensionless spin rates of $\Omega = 0.015, 0.030$ are used, similar to values used in the reference ARL simulations.[9] Motion covers $\phi = 360, 720$ deg of body rotation over a total time $t_{\text{final}} - \tau = 21T$ using $N = 100$ steps per convective time scale T. Figures 4–5 show example motion prescription and resulting aerodynamic load history for $\alpha_t = 20$ deg at the selected roll rates. For roll average, Equation (17), and roll damping, Equation (18), Figures 6–7 demonstrate the current results achieve good agreement with the reference wind tunnel and numerical data across the entire angle of attack range.
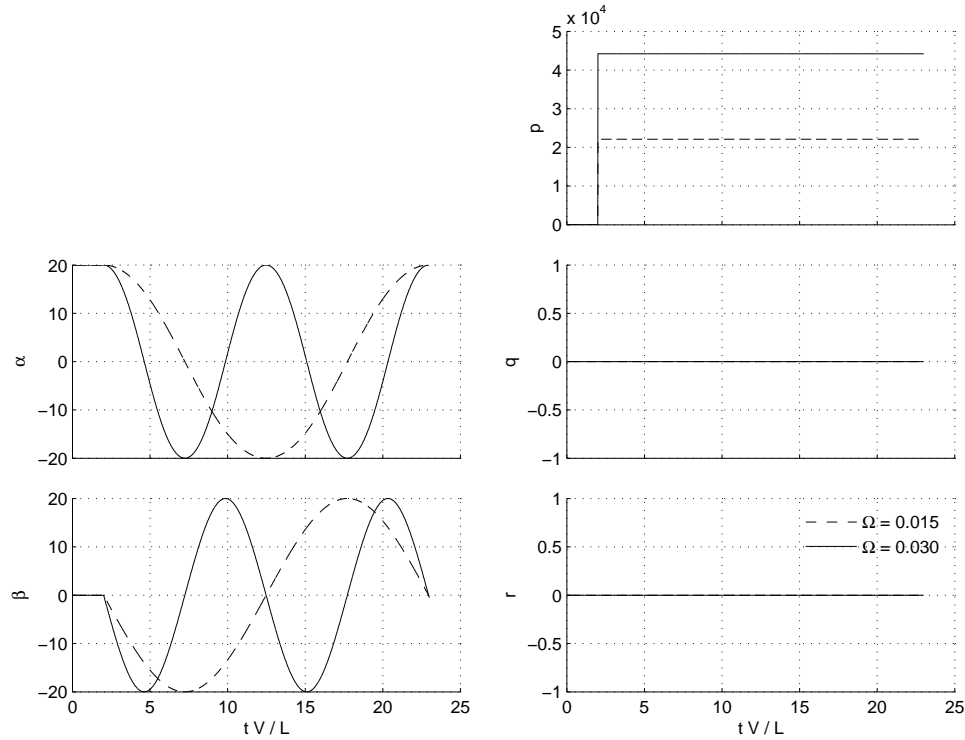
Figure 4: Example motion prescription for rolling airframe at $\alpha_t = 20$ deg.

III.B. Forced Harmonic Pitch

Consider sinusoidal motion in pitch such that

$$
\begin{aligned}
\alpha &= a_0 + A\sin(\omega t), \\
q &= \dot{\alpha} = \omega A\cos(\omega t), \\
\dot{q} &= \ddot{\alpha} = -\omega^2 A\sin(\omega t).
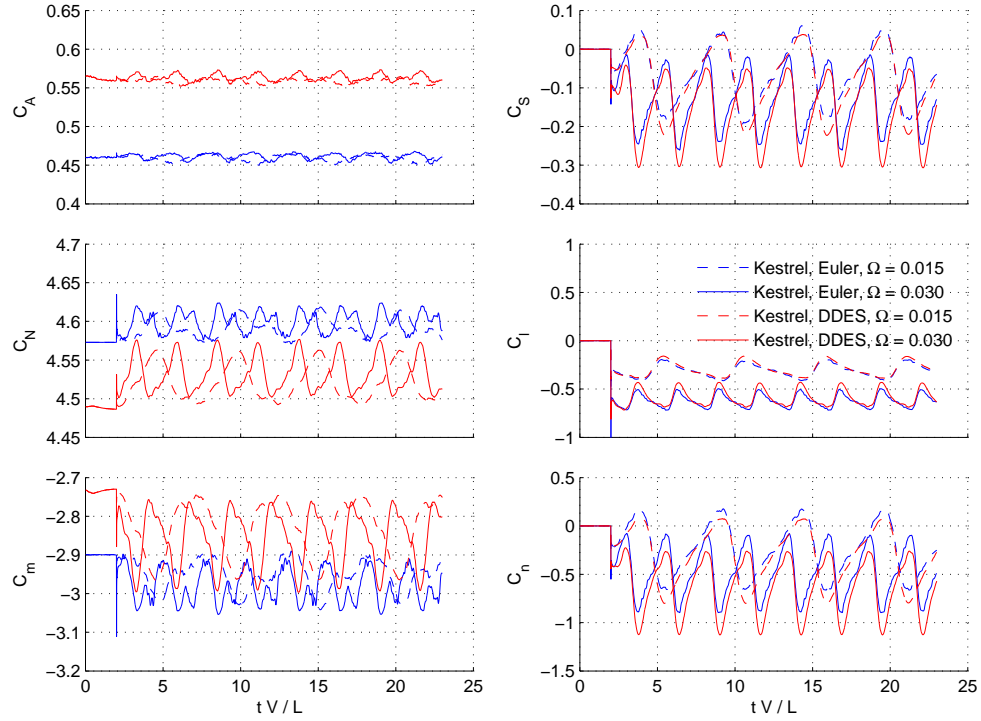\end{aligned}
\tag{20}
$$

Figure 5: Example aerodynamic loads history for rolling airframe at $\alpha_t = 20$ deg.
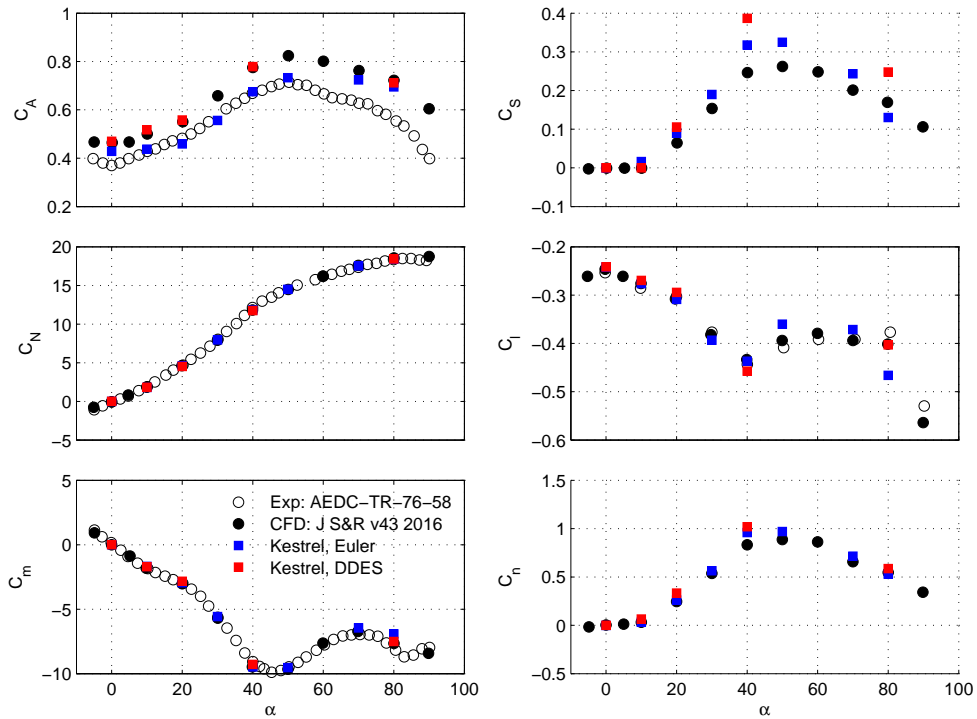

Figure 6: Comparison of current roll-averaged maneuver plane loads at $\Omega = 0.015$ with wind tunnel data[8] and reference CFD.[9]
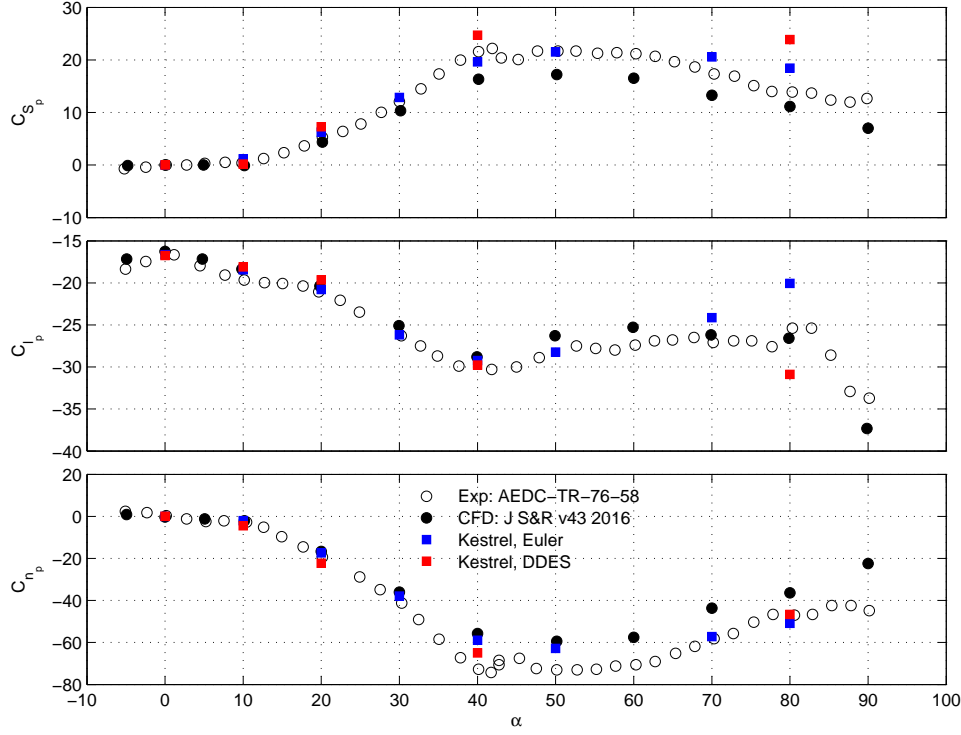
Figure 7: Comparison of current roll damping results with wind tunnel data[8] and reference CFD.[9]

With this motion prescription, Equation (2) becomes

$$C_m(t) = C_{m_0} + A(C_{m_\alpha} - k^2 C_{m_{\dot{q}}})\sin(\omega t) + Ak(C_{m_{\dot{\alpha}}} + C_{m_q})\cos(\omega t), \tag{21}$$

with the reduced frequency

$$k = \frac{\omega D}{2V}. \tag{22}$$

The pitch damping moment is then identified as the out-of-phase component

$$\bar{C}_{m_q} = C_{m_{\dot{\alpha}}} + C_{m_q}, \tag{23}$$

computed as the first Fourier coefficient of the response by

$$\bar{C}_{m_q} = \frac{2V}{n\pi AD} \int_{t_a}^{t_b} C_m(t)\cos(\omega t)\,\mathrm{d}t. \tag{24}$$

The period of integration $t_b - t_a = 2\pi n/\omega$ covers $n \geq 1$ integer number of cycles of motion and typically starts no sooner than the third cycle.

Example CFD solutions apply this scenario for comparing pitch damping with reference wind tunnel[6] and numerical[7] results. The motion prescription for forced oscillation in pitch is

$$\begin{aligned}
f_\alpha(t) &= A\sin(\omega(t-\tau))\,\mu(t-\tau), \\
f_q(t) &= \omega A\cos(\omega(t-\tau))\,\mu(t-\tau), \\
f_\beta(t) &= f_p(t) = f_r(t) = 0.
\end{aligned} \tag{25}$$

The motion amplitude is $A = (2V\sin A_\alpha)/(\omega L) \approx 0.32$ deg with $A_\alpha = 0.5$ deg and the reduced frequency is $k \approx 0.16$, similar to values used in the reference ARL simulations.[7] Motion covers three pitch cycles over $t_{\mathrm{final}} - \tau = 6T$ using $N = 200$ steps per convective timescale T. Figures 8–9 show example motion prescription and resulting aerodynamic load history for $\alpha_0 = 20$ deg at the selected amplitude and frequency. For pitch damping, Equation (24), Figure 10 shows good agreement between experiment and computation up to around $\alpha = 50$ deg. After this point, the reference wind tunnel data is very noisy, and the current computational results trend closely with the reference ARL CFD data.
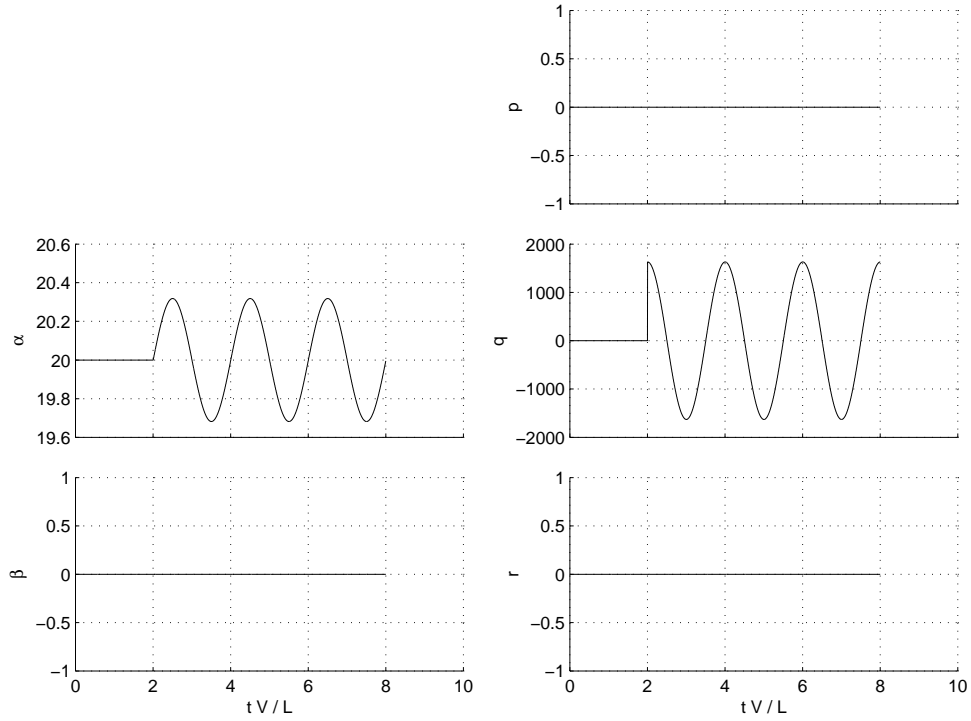
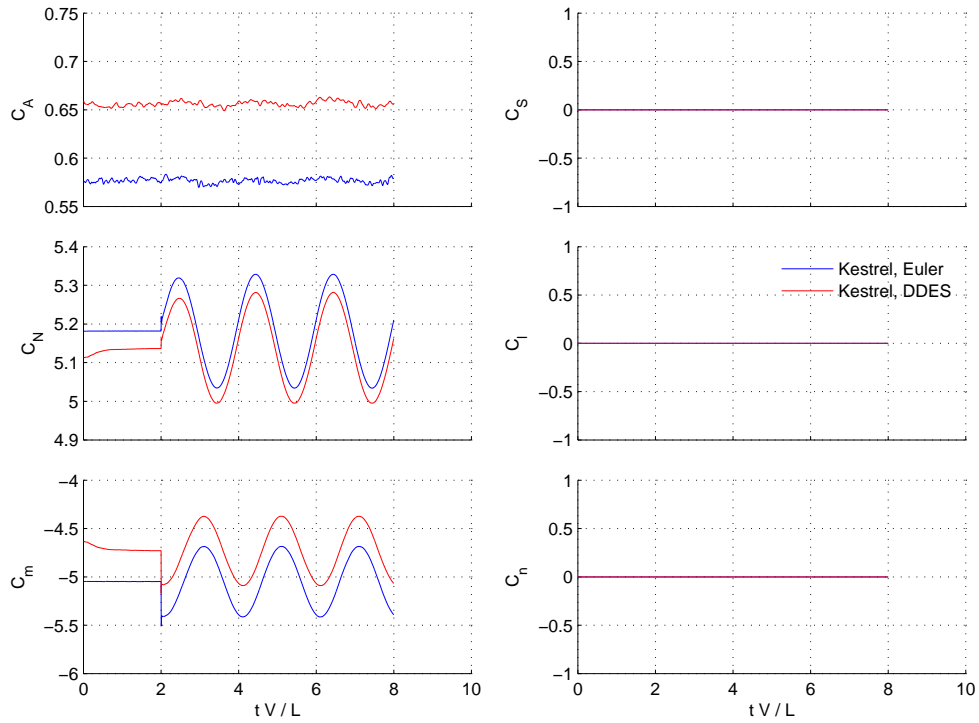Figure 8: Example motion prescription for harmonic motion in pitch about $\alpha_0 = 20$ deg.

Figure 9: Example aerodynamic loads history for harmonic motion in pitch about $\alpha_0 = 20$ deg.
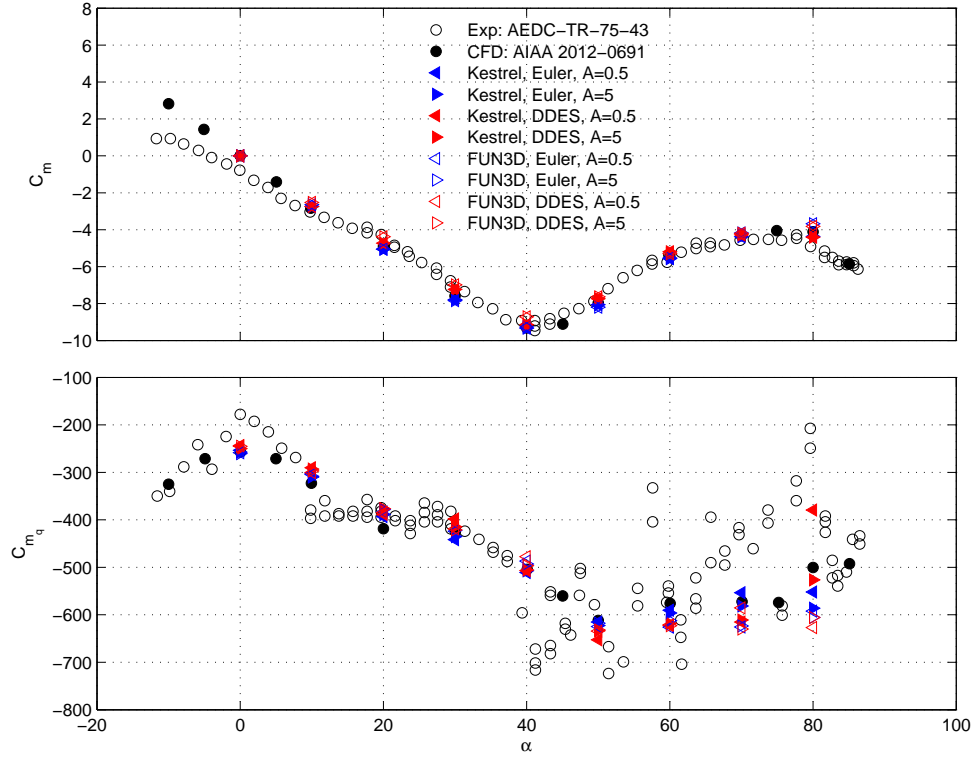
Figure 10: Comparison of current pitch damping results with wind tunnel data[6] and reference CFD.[7]

IV. Validation of Impulsive Motion

Linear time-invariant theory considers the response of a system to an arbitrary input signal. Most importantly, the fundamental result is that the system can be characterized completely with the impulse response. If an aerodynamic model training process can exploit that result by characterizing the input-output impulse relationship in one step, then computational efficiency may be gained over one-at-a-time exercises in harmonic and constant motion prescription above. The following development provides the essential notation and results to ultimately construct an aerodynamic state space model.

IV.A. Linear, Discrete Time, Time Invariant Dynamics

Let $h(k)$ denote the particular response of a linear system to the unit sample (impulse) sequence $\delta(k)$ defined by

$$\delta(k) = \begin{cases} 0 & \text{if } k \neq 0, \\ 1 & \text{if } k = 0. \end{cases} \tag{26}$$

The response of that linear system to the general forcing $u(k)$ is obtained by the convolution

$$y(k) = \sum_{i=-\infty}^{\infty} h(k-i)\,u(i) = \sum_{i=-\infty}^{\infty} h(i)\,u(k-i) = (u \star h)(k). \tag{27}$$

Similarly, let $S(k)$ denote the particular response of a linear system to the unit step sequence $\mu(k)$ defined by

$$\mu(k) = \begin{cases} 0 & \text{if } k < 0, \\ 1 & \text{if } k \geq 0. \end{cases} \tag{28}$$

The response of that linear system to the general forcing $u(k)$ is obtained by the convolution

$$y(k) = S(k)u(0) + \sum_{i=0}^{\infty} S(k-i)\frac{\mathrm{d}u}{\mathrm{d}t}(i)\,\Delta t. \tag{29}$$

For computational simplicity, it is preferred to use convolution with the actual input u rather than the derivative $\mathrm{d}u/\mathrm{d}t$. However, for practical reasons, it may also be preferred to excite the system with the unit step μ rather than the unit sample δ. Both of these desirables can be accommodated by noting that unit inputs are related via

$$\delta(k) = \mu(k) - \mu(k-1)\,, \quad \mu(k) = \sum_{i=0}^{\infty} \delta(k-i) = \sum_{i=-\infty}^{k} \delta(i), \tag{30}$$

and that the unit responses accordingly follow the same form as

$$h(k) = S(k) - S(k-1)\,, \quad S(k) = \sum_{i=0}^{\infty} h(k-i) = \sum_{i=-\infty}^{k} h(i). \tag{31}$$

Applying Equation (27) to pure longitudinal aerodynamics, for example, the unit translational response $h_{m,\alpha}$ and the unit rotational response $h_{m,q}$ are superposed as

$$C_m(k) = C_{m_0} + \sum_{i=0}^{\infty} h_{m,\alpha}(k)\,(\alpha(k-i) - \alpha_0) + \sum_{i=0}^{\infty} h_{m,q}(k)\frac{Dq(k-i)}{2V}. \tag{32}$$

Computing the normal force C_N by an analogous formula, the results are re-cast in the generic form

$$y(k) = \sum_{i=0}^{\infty} Y(i)\,u(k-i), \tag{33}$$

with measurement output vector, control input vector, and unit response matrices, respectively,

$$y(k) = \left\{ \begin{array}{c} C_N(k) - C_{N_0} \\ C_m(k) - C_{m_0} \end{array} \right\}\,, \quad u(k) = \left\{ \begin{array}{c} \alpha(k) - \alpha_0 \\ Dq(k)/2V \end{array} \right\}\,, \quad Y(k) = \begin{bmatrix} h_{N,\alpha}(k) & h_{N,q}(k) \\ h_{m,\alpha}(k) & h_{m,q}(k) \end{bmatrix}. \tag{34}$$

IV.B. Step Plunge and Step Rotation

The motion prescription for plunge (step change in α) is

$$\begin{aligned} f_\alpha(t) &= A_\alpha\,\mu(t-\tau), \\ f_\beta(t) &= f_p(t) = f_q(t) = f_r(t) = 0. \end{aligned} \tag{35}$$

with $A_\alpha = 0.5$ deg and the motion prescription for rotation (step change in q) is

$$\begin{aligned} f_q(t) &= A_q\,\mu(t-\tau), \\ f_\alpha(t) &= f_\beta(t) = f_p(t) = f_r(t) = 0, \end{aligned} \tag{36}$$

with $A_q = (2V/L)\sin A_\alpha$. Figures 11–12 and Figures 13–14 show example motion prescription and resulting aerodynamic load history for $\alpha_0 = 30$ deg at the selected amplitude. The step response of moment due to angle of attack and rotation rate are

$$S_{m,\alpha}(t) = \frac{C_m(t) - C_{m_0}}{A_\alpha}\,, \quad S_{m,q}(t) = \frac{C_m(t) - C_{m_0}}{DA_q/2V}, \tag{37}$$

and shown with their corresponding unit response $h_{m,\alpha}$ and $h_{m,q}$ in Figure 15. Note that both responses inherently contain a wide range of characteristic frequencies and quickly reach a steady state value after initiation.

The value of such solutions is that they may be used to predict any arbitrary motion of similar amplitude using superposition and convolution depicted in the Figure 16 (with notation shown as a classical Duhamel integral analogy to Equation 29.) This means that harmonic motion across a range of frequencies could be predicted with less computational expense than direct harmonic simulations. The relative error between convolution prediction and the direct CFD calculation of harmonic motion is $< 1\%$, which is negligible for pitch damping quantification. These results represent an intermediate step toward simultaneous impulse excitation of wind incidence angles and body rotation rates that can provide greater economy for aerodynamic damping prediction.
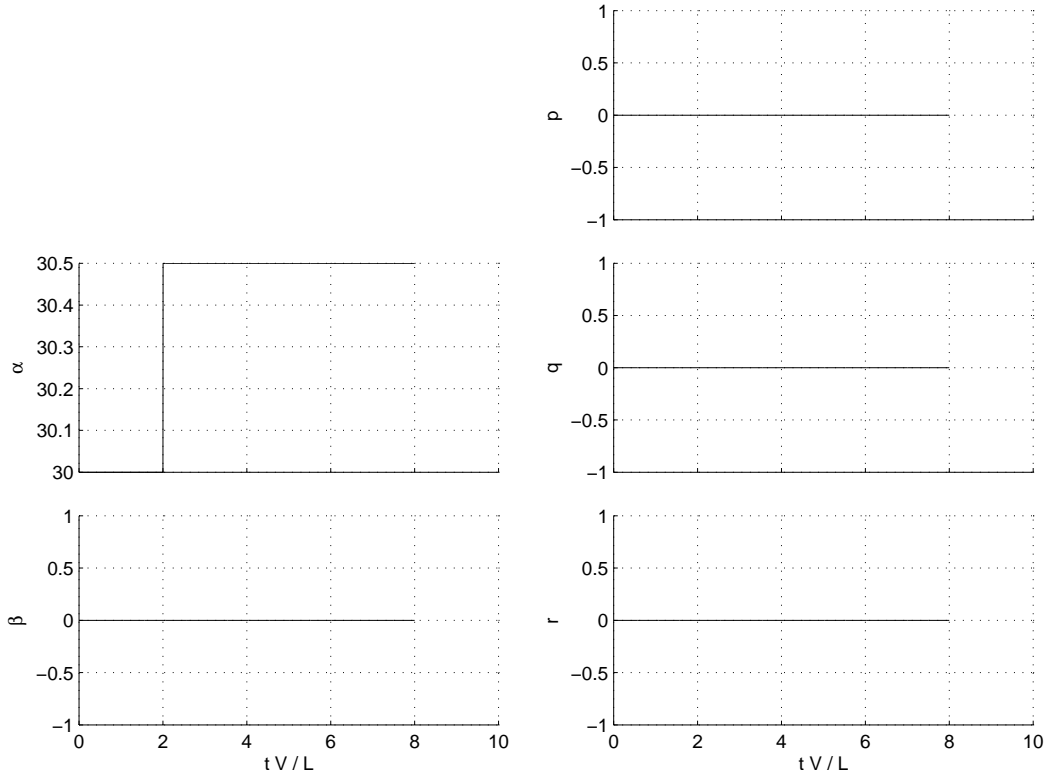
Figure 11: Example motion prescription for step change in translation rate at $\alpha_0 = 30$ deg.

IV.C. State Space Modeling and System Identification

Example CFD impulse solutions above demonstrate reconstruction of aerodynamic response to harmonic motion as a particular choice of general motion input. However, a model training exercise using that approach requires two separate runs (separate α and q) to identify the columns of the unit response matrices $Y(k)$. Therefore, a step towards computational efficiency requires a more sophisticated approach to compute the unit response matrices from a single run using simultaneous excitation of inputs. The following computational procedures directly follow Juang[10] and are implemented in the NASA System/Observer/Controller Identification Toolbox (SOCIT).

The linear, discrete time, time-invariant, finite dimensional model of a dynamical system can be represented as the discrete time state space model

$$\begin{aligned} x(k+1) &= Ax(k) + Bu(k), \\ y(k) &= Cx(k) + Du(k), \end{aligned} \tag{38}$$

where x is the n-dimensional state vector, y is the m-dimensional measurement output vector, and u is the r-dimensional control input vector. In this work, the input vector components are wind incidence angles and body rotation rates and the output vector components are aerodynamic coefficients. The state itself is
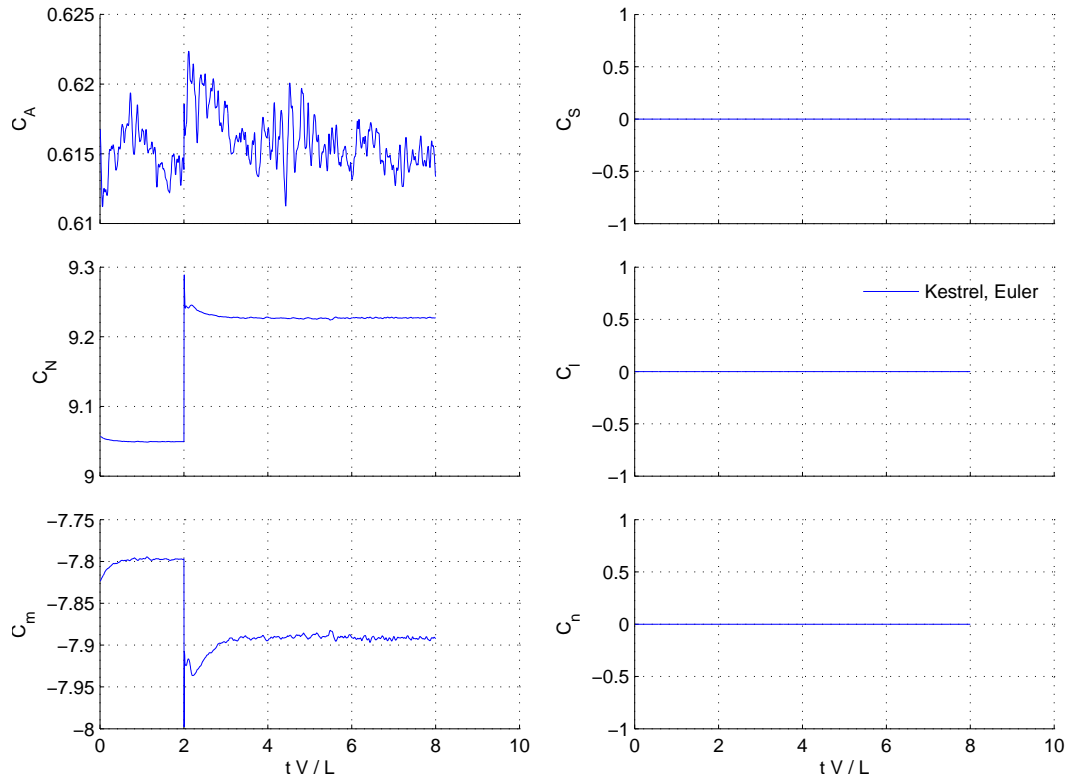
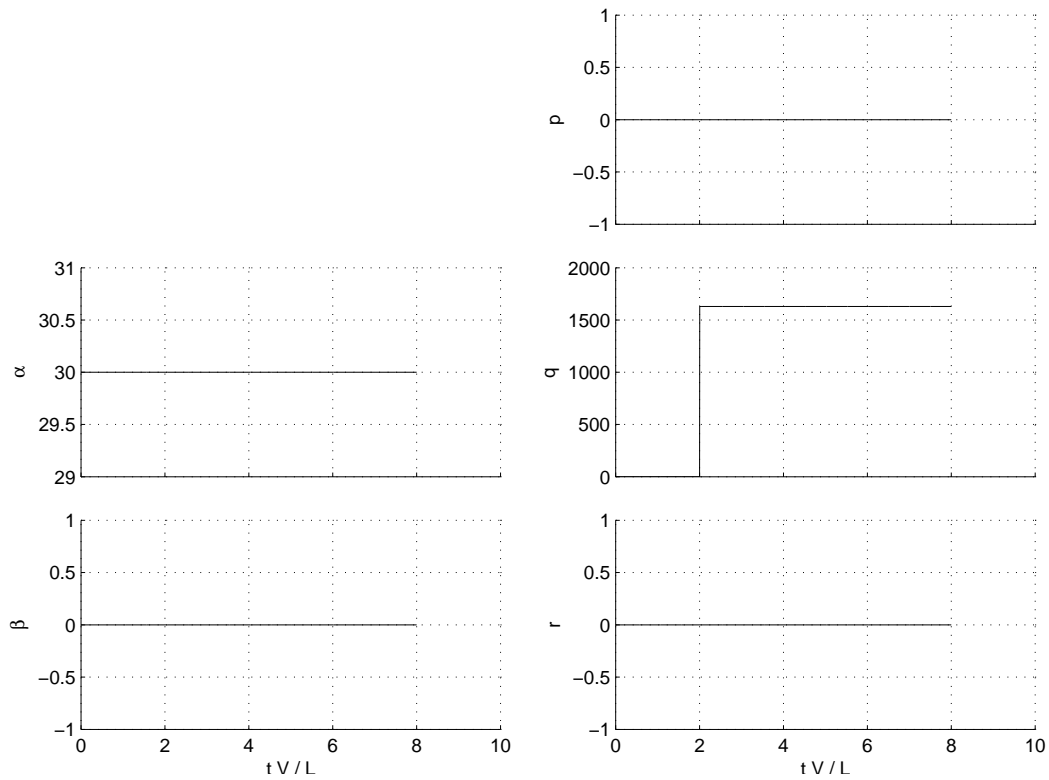Figure 12: Example aerodynamic loads history for step change in translation rate at $\alpha_0 = 30$ deg.

Figure 13: Example motion prescription for step change in rotation rate at $\alpha_0 = 30$ deg.

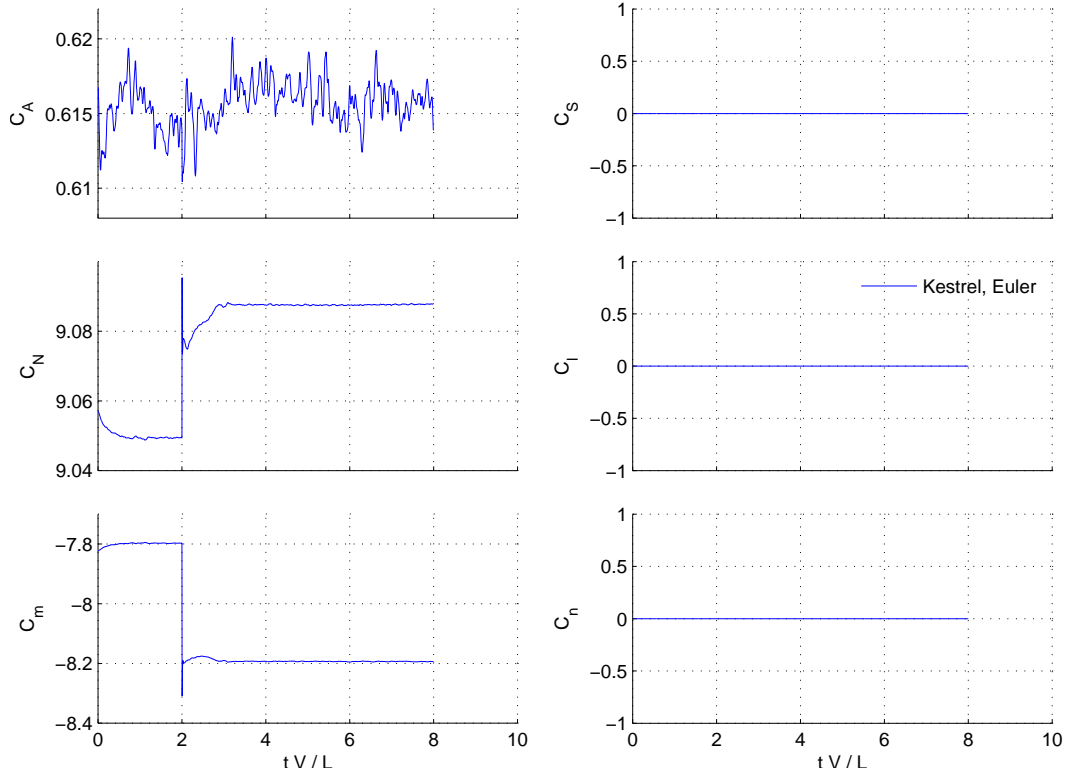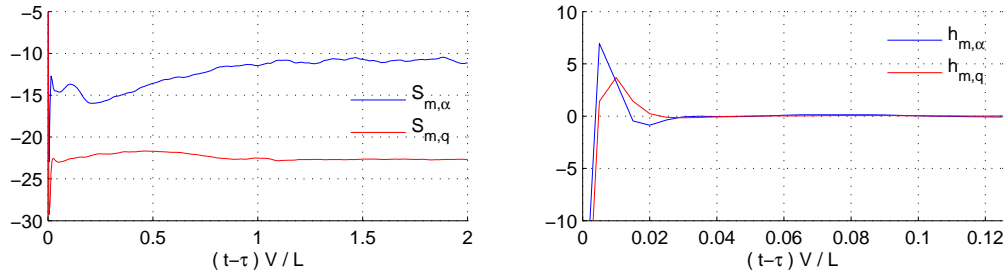American Institute of Aeronautics and Astronautics

Figure 14: Example aerodynamic loads history for step change in rotation rate at $\alpha_0 = 30$ deg.

Figure 15: Example moment step response and impulse response due to plunge and rotation at $\alpha_0 = 30$ deg.
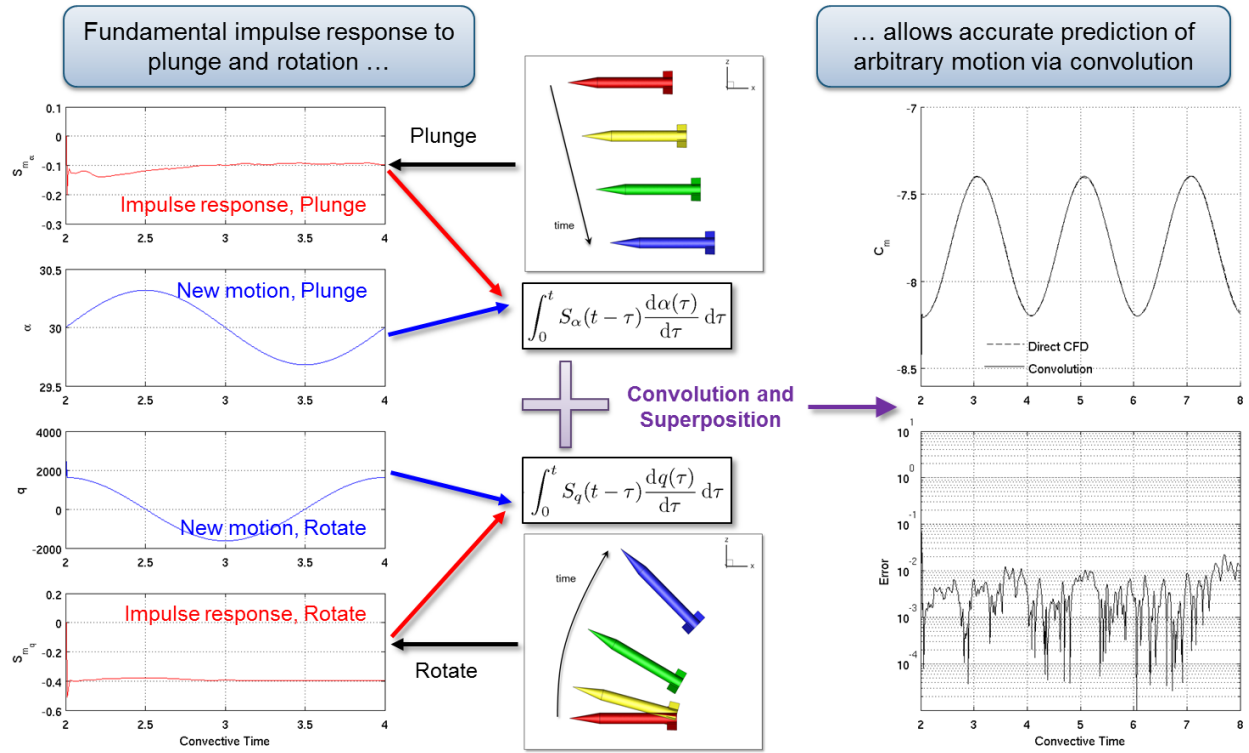
Figure 16: Process for superposition and convolution of system step response to produce general response to rigid body motion.

unknown. Solving Equation (38) with zero initial conditions on the state leads to

$$
\begin{aligned}
x(k) &= \sum_{i=1}^{k} A^{i-1} B\, u(k-i), \\
y(k) &= \sum_{i=1}^{k} C A^{i-1} B\, u(k-i) + D\, u(k).
\end{aligned}
\tag{39}
$$

In analogy to Equation 27, the system response, y, to general control input, u, is compactly written as the convolution

$$
y(k) = \sum_{i=0}^{k} Y(i)\, u(k-i),
\tag{40}
$$

with the $m \times r$ matrix Markov parameters identified as

$$
Y(k) = \begin{cases} D & \text{for } k = 0, \\ C A^{k-1} B & \text{for } k \geq 1. \end{cases}
\tag{41}
$$

Given known input-output data, the goal is to identify these Markov parameters and generate the constant system matrices A, B, C, D.

For the sequence $k = 0, 1, \ldots, l - 1$, grouping terms as

$$
\mathbf{y} = \begin{bmatrix} y(0) & y(1) & y(2) & \cdots & y(l-1) \end{bmatrix},
$$

$$
\mathbf{Y} = \begin{bmatrix} D & CB & CAB & \cdots & CA^{l-2}B \end{bmatrix},
$$

$$
\mathbf{U} = \begin{bmatrix} u(0) & u(1) & u(2) & \cdots & u(l-1) \\ & u(0) & u(1) & \cdots & u(l-2) \\ & & u(0) & \cdots & u(l-3) \\ & & & \ddots & \vdots \\ & & & & u(0) \end{bmatrix},
\tag{42}
$$

allows writing Equation (40) in the matrix form

$$
\mathbf{y} = \mathbf{Y}\mathbf{U}.
\tag{43}
$$

Unfortunately, inspection reveals that there are $m \times rl$ unknowns in the Markov parameter matrix but only $m \times l$ equations, limiting a unique solution only in the case of $r = 1$ control inputs. Furthermore, for zero control initial value, poor control frequency content, or large l, the matrix $\mathbf{U}$ becomes ill-conditioned and the matrix $\mathbf{Y}$ cannot be accurately computed from $\mathbf{Y} = \mathbf{y}\mathbf{U}^{-1}$.

Observer/Kalman Filter Identification (OKID) is an extension of the above formulation that allows for artificially increasing the system damping to improve numerical efficacy and efficiency, and for nonzero initial conditions. A term $Gy(k)$ is added and subtracted on the right hand side of the first of Equation (38) and terms are regrouped to yield the discrete time state space observer model

$$
\begin{aligned}
x(k+1) &= \bar{A}x(k) + \bar{B}v(k), \\
y(k) &= Cx(k) + Du(k),
\end{aligned}
\tag{44}
$$

where

$$
\begin{aligned}
\bar{A} &= A + GC, \\
\bar{B} &= \begin{bmatrix} B + GD, & -G \end{bmatrix}, \\
v(k) &= \begin{Bmatrix} u(k) \\ y(k) \end{Bmatrix}.
\end{aligned}
\tag{45}
$$

If the $n \times m$ matrix G is chosen to correspond to a deadbeat observer, then for some sufficiently large p, $C\bar{A}^k\bar{B} = 0$ for all time steps $k \geq p$. With zero initial conditions on the state, the input-output description is

$$
\mathbf{y} = \bar{\mathbf{Y}}\mathbf{V},
\tag{46}
$$

where

$$
\mathbf{y} = \begin{bmatrix} y(0) & y(1) & y(2) & \cdots & y(p) & \cdots & y(l-1) \end{bmatrix},
$$

$$
\bar{\mathbf{Y}} = \begin{bmatrix} D & C\bar{B} & C\bar{A}\bar{B} & \cdots & C\bar{A}^{p-1}\bar{B} \end{bmatrix},
$$

$$
\mathbf{V} = \begin{bmatrix} u(0) & u(1) & u(2) & \cdots & u(p) & \cdots & u(l-1) \\ & v(0) & v(1) & \cdots & v(p-1) & \cdots & v(l-2) \\ & & v(0) & \cdots & v(p-2) & \cdots & v(l-3) \\ & & & \ddots & \vdots & \cdots & \vdots \\ & & & & v(0) & \cdots & v(l-p-1) \end{bmatrix}.
\tag{47}
$$

A least squares solution of the observer Markov parameters is now possible:

$$
\bar{\mathbf{Y}} = \widetilde{\mathbf{y}}\widetilde{\mathbf{V}}^{\mathsf{T}} \left(\widetilde{\mathbf{V}}\widetilde{\mathbf{V}}^{\mathsf{T}} \right)^{-1}.
\tag{48}
$$

To recover the system Markov parameters $Y_k(A, B, C, D)$ from the observer Markov parameter matrix $\bar{\mathbf{Y}}$, partition the later as

$$\bar{\mathbf{Y}} = \begin{bmatrix} \bar{Y}_0 & \bar{Y}_1 & \cdots & \bar{Y}_p \end{bmatrix}, \quad \bar{Y}_k = \begin{bmatrix} \bar{Y}_k^{(1)} & -\bar{Y}_k^{(2)} \end{bmatrix} \quad \text{for } k = 1, \ldots, p, \tag{49}$$

and perform the recursion

$$\begin{aligned} Y_0 &= \bar{Y}_0 = D, \\ Y_k &= \bar{Y}_k^{(1)} - \sum_{i=1}^{k} \bar{Y}_i^{(2)} Y_{k-i} \quad \text{for } k = 1, \ldots, p. \end{aligned} \tag{50}$$

Similarly, to recover the observer gain Markov parameters $Y_k^o(G)$, perform the recursion

$$\begin{aligned} Y_1^o &= \bar{Y}_2 = CG, \\ Y_k^o &= \bar{Y}_k^{(2)} - \sum_{i=1}^{k-1} \bar{Y}_i^{(2)} Y_{k-i}^o \quad \text{for } k = 2, \ldots, p. \end{aligned} \tag{51}$$

The computational steps of OKID are found in Juang,[10] Figure 6.4, page 198.

The goal of system realization is to generate the constant system matrices A, B, C, D such that the output response of the given system due to a particular set of inputs is reproduced. Eigensystem Realization Algorithm (ERA) begins by forming the generalized $\alpha m \times \beta r$ Hankel matrix with $\alpha, \beta \geq n$ from the Markov parameters as

$$H(k-1) = \begin{bmatrix} Y(k) & Y(k+1) & \cdots & Y(k+\beta-1) \\ Y(k+1) & Y(k+2) & \cdots & Y(k+\beta) \\ \vdots & \vdots & \vdots & \ddots \\ Y(k+\alpha-1) & Y(k+\alpha) & \cdots & Y(k+\alpha+\beta-2) \end{bmatrix}. \tag{52}$$

The singular value decomposition yields

$$H(0) = R\,\Sigma\,S^\mathsf{T}. \tag{53}$$

Next, partition the decomposition according to the system order n (the number of "large enough" singular values) as

$$R = \begin{bmatrix} R_n & R_0 \end{bmatrix}, \quad \Sigma = \begin{bmatrix} \Sigma_n & 0 \\ 0 & \Sigma_0 \end{bmatrix}, \quad S = \begin{bmatrix} S_n & S_0 \end{bmatrix}. \tag{54}$$

Finally, compute the estimated system matrices by

$$\begin{aligned} \hat{A} &= \Sigma_n^{-1/2} R_n^\mathsf{T} H(1) S_n \Sigma_n^{-1/2}, \\ \hat{B} &= \Sigma_n^{1/2} S_n^\mathsf{T} E_r, \\ \hat{C} &= E_m^\mathsf{T} R_n \Sigma_n^{1/2}. \end{aligned} \tag{55}$$

where

$$\begin{aligned} E_m^\mathsf{T} &= \begin{bmatrix} I_m & O_m & \cdots & O_m \end{bmatrix}, \\ E_r^\mathsf{T} &= \begin{bmatrix} I_r & O_r & \cdots & O_r \end{bmatrix}. \end{aligned} \tag{56}$$

The computational steps of ERA are found in Juang,[10] Figure 5.3, page 153.

As pointed out by Silva,[18] excitation functions for state space model training should be based on the unit step for practical implementation and orthogonal for distinction within the SID process. The Walsh functions shown in Figure 17 are used for input excitation as they provide directional symmetry and embody the impulsive (beneficial) nature with regards to frequency bandwidth. Below, an example CFD solution with simultaneous excitation of all inputs demonstrates reconstruction of aerodynamic response to pitch plane harmonic motion. Obtained with a single run, the results are comparable to the impulse response superposition and convolution above and show no degradation from the out-of-plane inputs.
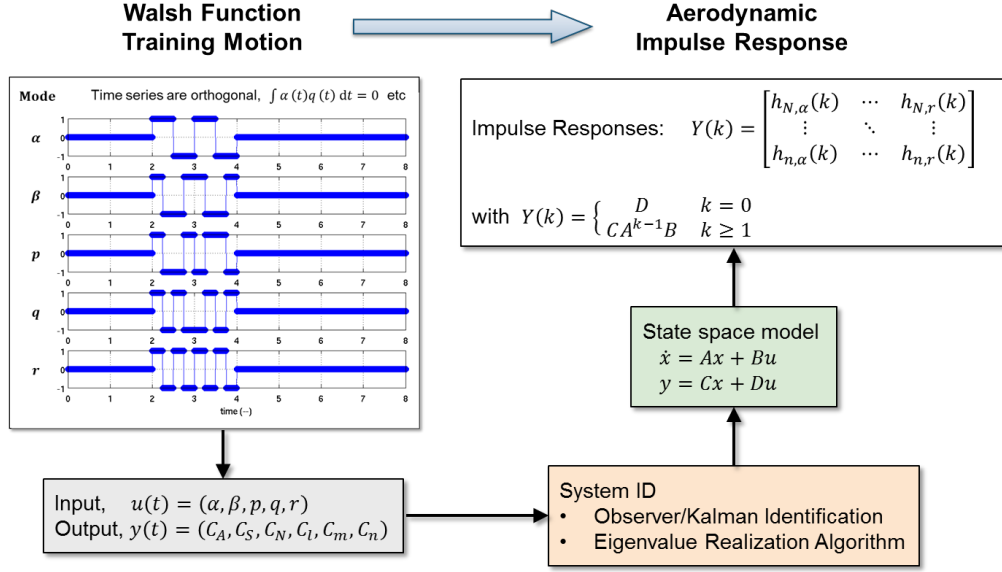
Figure 17: Generalization of impulse superposition and convolution using Walsh functions on rigid body motion inputs to identify a state space model.

IV.D. Concurrent Motion via Walsh Functions

The prescription for general impulsive motion is

$$
f_\alpha(t) = \sum_{i=1}^{I} A_{\alpha,i}\,\mu(t - \tau_{\alpha,i})\,, \quad f_\beta(t) = \sum_{i=1}^{I} A_{\beta,i}\,\mu(t - \tau_{\beta,i}),
$$
$$
f_p(t) = \sum_{i=1}^{I} A_{p,i}\,\mu(t - \tau_{p,i})\,, \quad f_q(t) = \sum_{i=1}^{I} A_{q,i}\,\mu(t - \tau_{q,i})\,, \quad f_r(t) = \sum_{i=1}^{I} A_{r,i}\,\mu(t - \tau_{r,i}),
$$

(57)

for some number of events I. In this work, motion prescription contains a maximum of $I = 16$ step events of minimum hold duration $T/2$, resulting in an excitation period of $t_{\text{final}} - \tau = 9T$. As before, there are $N = 200$ steps per convective timescale T. Amplitudes for wind incidence angles are $A_\alpha = A_\beta = 0.5$ deg and amplitudes for body rotation rates are $A_p = A_q = A_r = (2V/L)\sin A_\alpha$. Figures 18–19 show example motion prescription and resulting aerodynamic load history for $\alpha_0 = 10$ deg at the selected amplitudes and Walsh function frequency.

Given the motion prescription in the vector time history u and resulting aerodynamic load in the vector time history y, the SOCIT function `okid` provides the state space matrices A, B, C, D in Equation 38. Next, the corresponding input-output Markov parameters (analogous to the $h_{m,\alpha}, h_{m,q}$ above) are reconstructed according to Equation 41. Finally, the aerodynamic derivatives are computed according to Jenkins[1] as

$$
C_{m_\alpha} = S_{m,\alpha}(\infty) - S_{m,\alpha}(0)\,, \quad C_{m_q} = S_{m,q}(\infty) - S_{m,q}(0),
$$
$$
C_{m_{\dot\alpha}} = -\sum_{k=0}^{\infty} S_{m,\alpha}(\infty) - S_{m,\alpha}(k),
$$

(58)

where step and impulse response are related according to Equation 31. The entire process ultimately provides the pitch moment damping, $\bar{C}_{m_q} = C_{m_q} + C_{m_{\dot\alpha}}$, shown in Figure 20, plus 28 additional input-output relations $(\dim u \times \dim y = 30)$ not shown, within a single CFD run for each freestream α_0. For angles of attack $15 \leq \alpha_0 \leq 25$ deg, there appears to be disagreement among the various results, although an argument can be made that the experimental data specifically at $\alpha_0 = 10, 18, 25$ deg suggest that the damping is not actually constant across that range. Furthermore, and in contrast to harmonic motion training, the Walsh function motion training with SID results in much improved trends relative to experimental data for angles of attack $\alpha_0 \geq 25$ deg. Overall, these results represent an encouraging outcome towards the goal of efficient CFD-based construction of unsteady aerodynamic models.
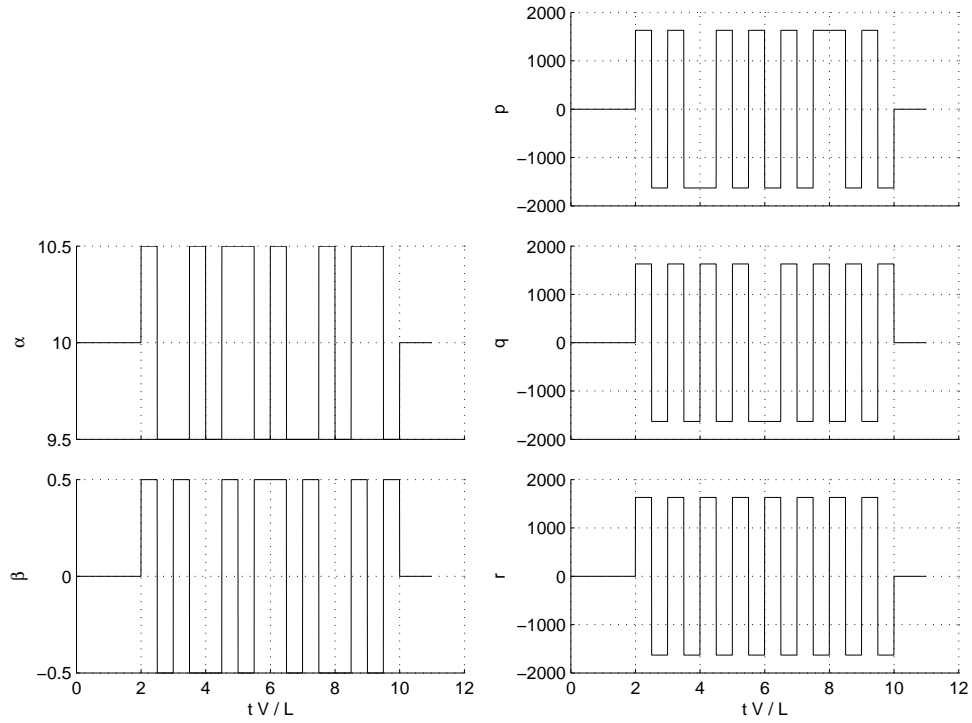
American Institute of Aeronautics and Astronautics

Figure 18: Example motion prescription with Walsh functions about $\alpha_0 = 10$ deg.
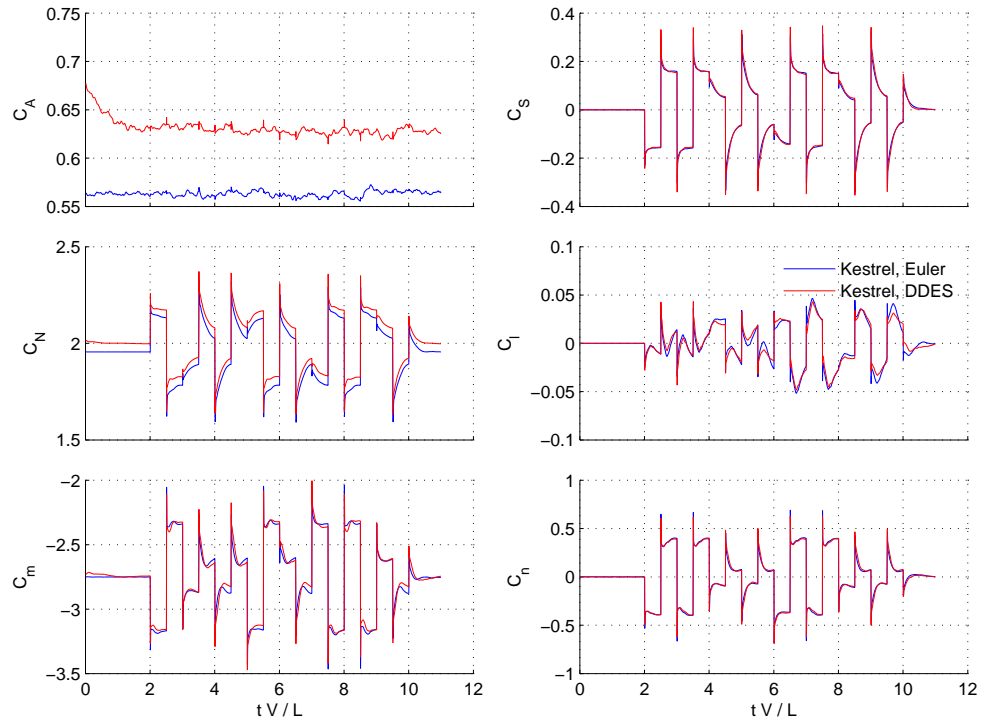
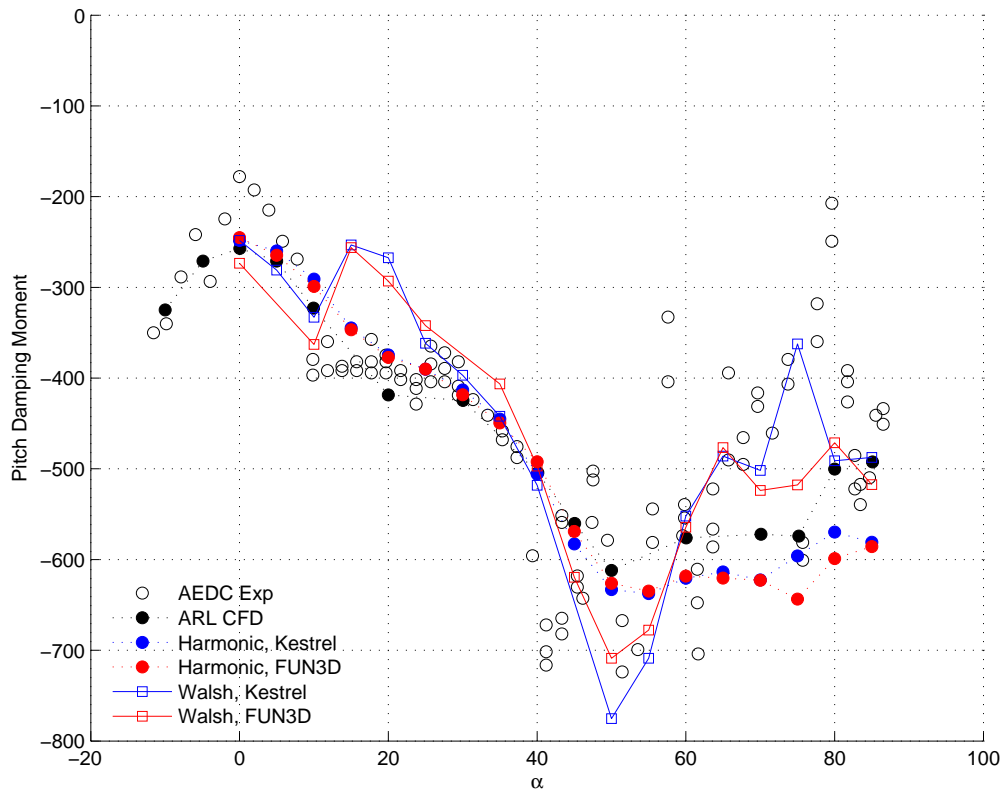Figure 19: Example aerodynamic loads history with Walsh functions about $\alpha_0 = 10$ deg.

American Institute of Aeronautics and Astronautics

Figure 20: Comparison of current pitch damping results with wind tunnel data[6] and reference CFD.[7]

V. Conclusions

This work considers a range of computational training maneuvers with system identification techniques to compute aerodynamic damping coefficients due to rigid body motion effects. The translation and rotation vectors of the airframe are governed by ODEs dependent on user-defined schedules of wind incidence angles (α, β) and body rotation rates (p, q, r). These are solved by numerical integration to obtain the particular data needed to drive time accurate CFD solutions with rigid body motion. In this way, the aerodynamic response to a variety of motions types from simple harmonic pitch to simultaneous input impulse are computed.

Using the Army-Navy Finner geometry, the first activity focuses on comparison of current harmonic pitch (sinusoidal $q = \dot{\alpha}$) and steady roll (constant p) computations to reference wind tunnel (AEDC) and computational fluid dynamics (ARL) data at $M \approx 2$ and $0 \leq \alpha \leq 90$ deg. Current results show good agreement to the reference data. Next, example solutions for plunge (step change in α) and rotation (step change in q) provide fundamental aerodynamic characterization about a reference state. Using the classical linear, time-invariant system dynamics concepts of superposition and convolution, the results demonstrate successful aerodynamic prediction of subsequent arbitrary motion. Finally, as generalization of the superposition and convolution concepts, SOCIT generates state space aerodynamic models using multiple, Walsh function scheduled, rigid body mode inputs for multiple aerodynamic outputs. Again, the results demonstrate a successful aerodynamic prediction of subsequent pitch plane harmonic motion free of any degradation from out-of-plane input data. With fewer and shorter CFD runs that collect all of the unsteady input-output relationship at once, this approach promises to greatly economize the CFD-based training process for aerodynamic damping modeling.

For future work, we recommend a detailed parameter study for the example problems reported here. For the harmonic motion, these include amplitude, frequency, timestep, and motion duration. For the Walsh function scheduled motion, these include amplitude (related to linearization), timestep (related to high frequency content), minimum event hold (related to economy), total excitation period (related to low frequency content), and SOCIT user parameters. Additionally, we recommend applying the above computational processes to a suitable airplane-like geometry to elucidate yaw damping and yaw-roll coupling. An ideal configuration would be geometrically simple like the AGARD-C and have aerodynamic damping wind tunnel data. The simultaneous input approach on a non-rotationally symmetric geometry would allow us to more thoroughly exercise the resulting state space model for all aerodynamic coefficients.

Acknowledgements

References

[1] Jenkins, J., "Dynamic Stability Derivatives," Tech. Rep. AFRL-RQ-WP-TR-2015-0141, Air Force Research Laboratory, 2015.

[2] Da Ronch, A., Vallespin, D., Ghoreyshi, M., and Badcock, K., "Computation of dynamic derivatives using CFD," *Applied Aerodynamics Conference*, AIAA Paper 2010-4817, Chicago, IL, June 2010.

[3] Da Ronch, A., McCracken, A., Badcock, K., Ghoreyshi, M., and Cummings, R., "Modeling of unsteady aerodynamic loads," *Atmospheric Flight Mechanics Conference*, AIAA Paper 2011-6524, Portland, OR, August 2011.

[4] Ghoreyshi, M., Jirásek, A., and Cummings, R., "Reduced order unsteady aerodynamic modeling for stability and control analysis using computational fluid dynamics," *Progress in Aerospace Sciences*, Vol. 71, 2014, pp. 167–217.

[5] Ghoreyshi, M., Badcock, K., Da Ronch, A., Marqyes, S., and Ames, N., "Framework for establishing limits of tabular aerodynamic models for flight dynamics analysis," *Journal of Aircraft*, Vol. 48, 2011, pp. 42–55.

[6] Uselton, R. and Uselton, J., "Test mechanism for measuring pitch-damping derivatives of missile configurations at high angles of attack," Tech. Rep. AEDC-TR-75-43, Arnold Engineering Development Center, 1975.

[7] Bhagwandin, V. and J.Sahu, "Numerical prediction of pitch damping derivatives for a finned projectile at angles of attack," *50th Aerospace Sciences Meeting*, AIAA Paper 2012-0691, Nashville, TN, January 2012.

[8] Jenke, L., "Experimental roll-damping, Magnus, and static-stability characteristics of two slender missile configurations

at high angles of attack [0 to 90 deg] and Mach numbers 0.2 through 2.5," Tech. Rep. AEDC-TR-76-58, Arnold Engineering Development Center, 1976.

[9]Bhagwandin, V., "High-alpha prediction of roll damping and Magnus coefficients for finned projectiles," *Journal of Spacecraft and Rockets*, Vol. 53, 2016, pp. 710–729.

[10]Juang, J.-N., *Applied System Identification*, Prentice-Hall, 1994.

[11]Zipfel, P., *Modeling and simulation of aerospace vehicle dynamics*, American Institute of Aeronautics and Astronautics, 2nd ed., 2007.

[12]Etkin, B., *Dynamics of Flight*, John Wiley & Sons, 2nd ed., 1982.

[13]Stevens, B. and Lewis, F., *Aircraft Control and Simulation*, John Wiley & Sons, 2nd ed., 2003.

[14]Dey, S., "Capstone: A platform for geometry, mesh and attribution modeling for physics-based analysis and design," *NDIA Physics-Based Modeling in Design and Development for US Defense Conference*, Denver, CO, November 2011.

[15]Morton, S. and McDaniel, D., "HPCMP CREATE-AV Kestrel Current Capabilities and Future Direction for Fixed Wing Aircraft Simulations," *50th Aerospace Sciences Meeting*, AIAA Paper 2015-0039, Kissimmee, FL, January 2015.

[16]Biedron, R., Carlson, J., Derlaga, J., Gnoffo, P., Hammond, D., Jones, W., Kleb, B., Lee-Rausch, E., Nielsen, E., Park, M., Rumsey, C., Thomas, J., and Wood, W., "FUN3D Manual: 12.9," Tech. Rep. TM-2016-219330, National Aeronautics and Space Administration, 2016.

[17]Cummings, R., Morton, S., and McDaniel, D., "Experiences in accurately predicting time-dependent flows," *Progress in Aerospace Sciences*, Vol. 44, 2008, pp. 241–257.

[18]Silva, W., "Simultaneous excitation of multiple input / multiple output CFD-based unsteady aerodynamic systems," *Journal of Aircraft*, Vol. 45, 2003, pp. 1267–1274.